A Periodic DFT Study of Intramolecular Isomerization Reactions of Toluene and Xylenes Catalyzed by Acidic Mordenite

Xavier Rozanska,*,† Rutger A. van Santen,† François Hutschka,‡ and Juergen Hafner§

Contribution from the Schuit Institute of Catalysis, Laboratory of Inorganic Chemistry and Catalysis, Eindhoven University of Technology, P.O. Box 513, 5600 MB Eindhoven, The Netherlands, TotalFina, Centre Européen de Recherche et Technique, Département Chimie des Procédés, B.P. 27, 76700 Harfleur, France, and Institut für Materialphysik, Universität Wien, Sensengasse 8, A-1090 Wien, Austria

Received February 12, 2001. Revised Manuscript Received May 31, 2001

Abstract: A periodic density functional theory (DFT) study of the isomerization reactions of toluene and xylene catalyzed by acidic mordenite is reported. Monomolecular isomerization reactions have been considered and analyzed. The different reaction pathways have been discussed in detail. The use of periodic structure calculations allows consideration and analysis of zeolite electrostatic contributions and steric constraints that occur within zeolite micropores. Major differences in the details of protonation reaction pathways are found when periodic structures are used rather than small cluster models of the Brønsted acidic site. Complex relationships are found between zeolite topology and reaction pathways.

1. Introduction

Zeolites are natural or synthetic silicon oxide crystals composed of a network of SiO_4 tetrahedral units which link together by sharing oxygen atoms.[1] The potential energy surface of the zeolite Si−O−Si angles is rather flat[1e] which explains the large variety of accessible micropore structures that can be formed by zeolites. Zeolites have well-defined microporous structures, which make them interesting agents for separation purposes.[1b,d,2] Moreover, their mechanical and thermal properties have given them an important position in heterogeneous catalysis.[3] In addition, zeolite-catalyzed reactions often display high product selectivity.[4] The selectivity finds its source in the zeolite micropore structure with different consequences on the course of a reaction.

A first, rather obvious, reason is the reactant selectivity. As the zeolite micropore channels have a well-defined diameter, reactants bigger than this diameter cannot enter the micropores in order to react. Reactants smaller than the micropores will be the only ones to get involved in reactions.

Once a reactant molecule has adsorbed within the zeolite mouth, it needs to diffuse toward the active sites where reactions will occur. This diffusion can be very dependent upon the size and shape of the zeolite micropores as well as on the size of the reactants or products. After reaction has occurred, the products must diffuse away from the micropores.

These selective properties are not only valid in the case of zeolite catalysts but also in the case of zeolite molecular sieves.

After reactants have adsorbed within the zeolite mouth and diffused toward the actives sites, they must adsorb. Selective adsorption can occur as a result of the local topology of the active site, its immediate surroundings, and the reactant. This selective adsorption of the reactants to the active sites results in preferential reaction pathways.

Reaction transition states require specific geometry so that reaction may proceed. They can be hampered or prohibited by the available space around the catalytic active site.[4] This effect is designated as transition-state selectivity.

Selective diffusion of products and reactants can be better investigated using classical dynamic or Monte Carlo simulations,[5] or experimental techniques,[1c,6] because of the time scale of the processes. Quantum chemical calculations are required to analyze molecular reactivity.

Quantum chemical periodic electronic structure calculations provide an efficient way to describe the interaction between guest molecules and the zeolite framework. The quantum-chemical periodic structure codes have recently become even more useful, since it has become possible to localize ap-

* Address correspondence to this author. Fax: +31 40 245 5054. E-mail: tgakxr@chem.tue.nl.

† Schuit Institute of Catalysis.

‡ Centre Européen de Recherche et Technique. TotalFina.

§ Universität Wien.

(1) (a) Breck, D. *Zeolite Molecular Sieves, Structure, Chemistry and Use*; Wiley: New York, 1974. (b) Barrer, R. M. *Zeolite and Clay Minerals as Sorbents and Molecular Sieves*; Academic Press: New York, 1978. (c) Jobic, H. *Spectrochim. Acta* **1992**, *48A*, 293−312. (d) Fricke, R.; Kosslick, H.; Lischke, G.; Richter, M. *Chem. Rev.* **2000**, *100*, 2303−2405. (e) Van Santen, R. A.; Kramer, G. J. *Chem. Rev.* **1995**, *95*, 637−660.

(2) Chen, N. Y.; Degnan, T. F., Jr.; Smith, C. M. *Molecular Transport and Reaction in Zeolites, Design and Application of Shape Selective Catalyst*; VCH Publishers: New York, 1994; pp 173−193.

(3) Ertl, G.; Knözinger, H.; Weitkamp, J. *Handbook of Heterogeneous Catalysis*; Wiley-VCH: Weinheim, 1997.

(4) (a) Csicsery, S. M. *Zeolites* **1984**, *4*, 202−213. (b) Fraenkel, D.; Levy, M. *J. Catal.* **1989**, *118*, 10−21. (c) Chen, N. Y.; Degnan, T. F., Jr.; Smith, C. M. *Molecular Transport and Reaction in Zeolites, Design and Application of Shape Selective Catalyst*; VCH Publishers: New York, 1994; pp 195−289. (d) Venuto, P. B. *Microporous Mater.* **1994**, *2*, 297−411. (e) Tsai, T.-C.; Liu, S.-B.; Wang, I. *Appl. Catal. A* **1999**, *181*, 355−398.

(5) (a) Frenkel, D. *Proceeding of the Euroconference on Computer Simulation in Condensed Matter Physics and Chemistry, Como 1995*; Binder, K., Ciccotti, A., Eds.; Italian Physical Society: Bologna, 1995; Chapter 7. (b) Schuring, D.; Jansen, A. P. J.; Van Santen, R. A. *J. Phys. Chem. B* **2000**, *104*, 941−948. (c) Smit, B.; Siepmann, J. I. *J. Phys. Chem.* **1994**, *98*, 8442−8452. (d) Smit, B. *Mol. Phys.* **1995**, *85*, 153−172. (e) Smit, B.; Maesen, T. L. M. *Nature* **1995**, *374*, 42−44.

(6) Schumacher, R. R.; Anderson, B. G.; Noordhoek, N. J.; De Gauw, F. J. M. M.; De Jong, A. M.; De Voigt, M. J. A.; Van Santen, R. A. *Microporous Mesoporous Mater.* **2000**, *35−36*, 315−326.

10.1021/ja0103795 CCC: $20.00
Published on Web 07/14/2001

proximate transition structures. This allows us to investigate the effect of the zeolite framework on the course of a reaction.

In the zeolite framework, tetravalent silicon atoms of zeolite crystals can be substituted with trivalent atoms such as Al^{III}.[1−4] A cation has to be introduced at the same time to neutralize the resulting negative framework charge. When the cation is a proton, zeolites can act as solid acid catalysts. Such catalysts are obtained when the M^+ cation of a $M_x[Al_xSi_{1-x}O_2]\cdot nH_2O$ zeolite is ion-exchanged with NH_4^+. The heating of the NH_4^+-exchanged zeolite induces NH_3 to desorb, and a proton is left behind. The proton binds to an oxygen atom that bridges an aluminum atom and a silicon atom.

Contrary to homogeneous acids that organize their molecules around charged species,[7] zeolite frameworks have a limited flexibility and cannot significantly alter their geometry in the presence of strongly interacting charged species.[8] Besides being ionic crystals, zeolites are characterized by a small dielectric constant (ϵ around 5)[9] and show important Coulombic charge screening.[10] In the case of olefins adsorbed within zeolites, short-range electrostatic interactions, such as dispersion, ion−quadrupole interaction and induced electrostatic interaction contribute for up to 84% of the adsorption energy.[10c] These properties make it impossible for protonated hydrocarbon molecules to exist as stable "free" charged species within zeolite micropores.[1e,11] Instead, protonation reactions of hydrocarbons lead to chemisorption with the formation of alkoxy or σ-bonded species.[11] On the other hand, it is now well understood that hydrocarbon reactions catalyzed by acidic zeolites involve transition states of an ionic nature.[1−4,12] Quantum chemical periodic structure calculations give us the opportunity to investigate in a realistic way the effect of the zeolite bulk electrostatic contribution on transition states.

The isomerization reaction of xylene isomers catalyzed by acidic zeolites shows a selectivity in favor of *para*-xylene.[2−4,13−15] This xylene isomer is a more valuable product than *meta*- or *ortho*-xylene as it is an important intermediate for terphthalic acid, an important polymer monomer.[4e] In the first part of this paper, the toluene isomerization reaction will be considered. Isomerization reaction pathways of toluene will be extensively investigated and will provide a basis for the study of the reaction pathways of xylene isomers, to be discussed in next section.

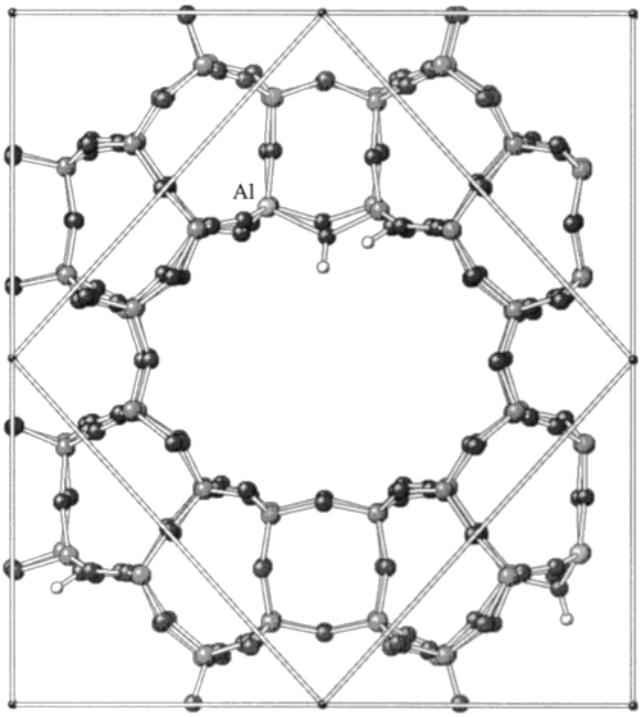

Figure 1. Mordenite zeolite. This zeolite is characterized by large parallel 12-membered rings that have smaller 8-membered ring side pockets. It belongs to the class of the large micropore zeolites.

The intramolecular isomerization reactions of toluene and xylenes catalyzed by acidic mordenite (H-MOR) will be analyzed in detail. Next to faujasite and ZSM-5, mordenite (MOR) is one of the most commonly commercially used zeolites in catalysis (see Figure 1).[1−4] We have chosen mordenite because the small unit cell facilitates the calculations. Mordenite has two sets of intersecting channels: large channels subscribed by 12 T-atoms that are straight and have a free diameter of 6.5 × 7.0 Å, and small side pocket channels subscribed by 8 T-atoms and oriented perpendicularly to the main channel and that have a free diameter of 2.6 × 5.7 Å. It has been shown that aromatics isomerization catalyzed by acidic mordenite occurs mainly via monomolecular processes (see Scheme 1).[13] The intermolecular isomerization of aromatics within mordenite is hampered by steric constraints and will therefore not be considered. Despite the experimental[4d,13−15] and theoretical[16] demonstrations that intermolecular mechanisms are favored over monomolecular isomerization, this reaction pathway is suppressed in mordenite since it involves a diphenylmethane intermediate that cannot fit easily in the straight channels of MOR.[13] It is well-known that transition-state selectivity alone cannot explain *para*-xylene selectivity in acidic zeolite catalysts.[17] It has been shown that product diffusivity plays also an important role in the selectivity of the isomerization reactions

(7) Kazansky, V. B. *Top. Catal.* **2000**, *11*−*12*, 55−60.

(8) (a) Kramer, G. J.; De Man, A. J. M.; Van Santen, R. A. *J. Am. Chem. Soc.* **1991**, *113*, 6435−6441. (b) Ugliengo, P.; Civalleri, B.; Zicovich-Wilson, C. M.; Dovesi, R. *Chem. Phys. Lett.* **2000**, *318*, 247−255. (c) Brändle, M.; Sauer, J.; Dovesi, R.; Harrison, N. M. *J. Chem. Phys.* **1998**, *109*, 10379−10389.

(9) (a) De Man, A. J. M.; Van Beest, B. M. W.; Leslie, M.; Van Santen, R. A. *J. Phys. Chem.* **1990**, *94*, 2524−2534. (b) Schröder, K.-P.; Sauer, J. *J. Phys. Chem.* **1996**, *100*, 11043−11049.

(10) (a) Lee, C.; Parrillo, D. J.; Gorte, R. J.; Farneth, W. E. *J. Am. Chem. Soc.* **1996**, *118*, 3262−3268. (b) Gourseot, A.; Arbuznikov, A.; Vasilyev, V. *Density Functional Theory, a Bridge Between Chemistry and Physics*; Geerlings, P., De Proft, F., Langenaeker, W., Eds.; VUB University Press: Brussels, 1999; pp 155−168. (c) Zhen, S.; Seff, K. *Microporous Mesoporous Mater.* **2000**, *39*, 1−18.

(11) (a) Haw, J. F.; Richardson, B. R.; Oshiro, I. S.; Lazo, N. D.; Speed, J. A. *J. Am. Chem. Soc.* **1989**, *111*, 2052−2058. (b) Kazansky, V. B.; Senchenya, I. N. *J. Catal.* **1989**, *119*, 108−120. (c) Haw, J. F.; Nicholas, J. B.; Xu, T.; Beck, L. W.; Ferguson, D. B. *Acc. Chem. Res.* **1996**, *29*, 259−267. (d) Paukshtis, E. A.; Malysheva, L. V.; Stepanov, V. G. *React. Kinet. Catal. Lett.* **1998**, *65*, 145−152.

(12) (a) Boronat, M.; Viruela, P.; Corma, A. *J. Phys. Chem. A* **1998**, *102*, 982−989. (b) Frash, M. V.; Van Santen, R. A. *Top. Catal.* **1999**, *9*, 191−205. (c) Sauer, J.; Sierka, M.; Haase, F. *Transition State Modeling for Catalysis*; Truhlar, D. G., Morokuma, K., Eds.; ACS Symposium Series 721; American Chemical Society: Washington, DC, 1999; pp 358−367. (d) Zygmunt, S. A.; Curtiss, L. A.; Zapol, P.; Iton, L. E. *J. Phys. Chem. B* **2000**, *104*, 1944−1949.

(13) (a) Corma, A.; Sastre, E. *J. Catal.* **1991**, *129*, 177−185. (b) Halgeri, A. B.; Das, J. *Appl. Catal., A* **1999**, *181*, 347−354.

(14) Gnep, N. S.; Tejada, J.; Guisnet, M. *Bull. Soc. Chim. Fr.* **1982**, *1*−*2*, I4−I11.

(15) (a) Lanewala, M. A.; Bolton, A. P. *J. Org. Chem.* **1969**, *34*, 3107−3112. (b) Young, L. B.; Butter, S. A.; Kaeding, W. W. *J. Catal.* **1982**, *76*, 418−432. (c) Guisnet, M.; Gnep, N. S.; Morin, S. *Microporous Mesoporous Mater.* **2000**, *35*−*36*, 47−59.

(16) (a) Blaszkowsky, S. R.; Van Santen, R. A. *Transition State Modeling for Catalysis*; Truhlar, D. G., Morokuma, K., Eds.; ACS Symposium Series 721; American Chemical Society: Washington, DC, 1999; Chapter 20. (b) Rozanska, X.; Saintigny, X.; Van Santen, R. A.; Hutschka, F. *J. Catal.* In press. (c) Corma, A.; Sastre, G.; Viruela, P. M. *J. Mol. Catal. A* **1995**, *100*, 75−85.

(17) (a) Mirth, G.; Cejka, J.; Lercher, J. A. *J. Catal.* **1993**, *139*, 24−33. (b) Mirth, G.; Lercher, J. A. *J. Catal.* **1994**, *147*, 199−206.

Scheme 1. Reaction Mechanisms of the Intra and Inter Isomerizations of Aromatics Catalyzed by Acidic Zeolite[4d,e,15,16] *a*

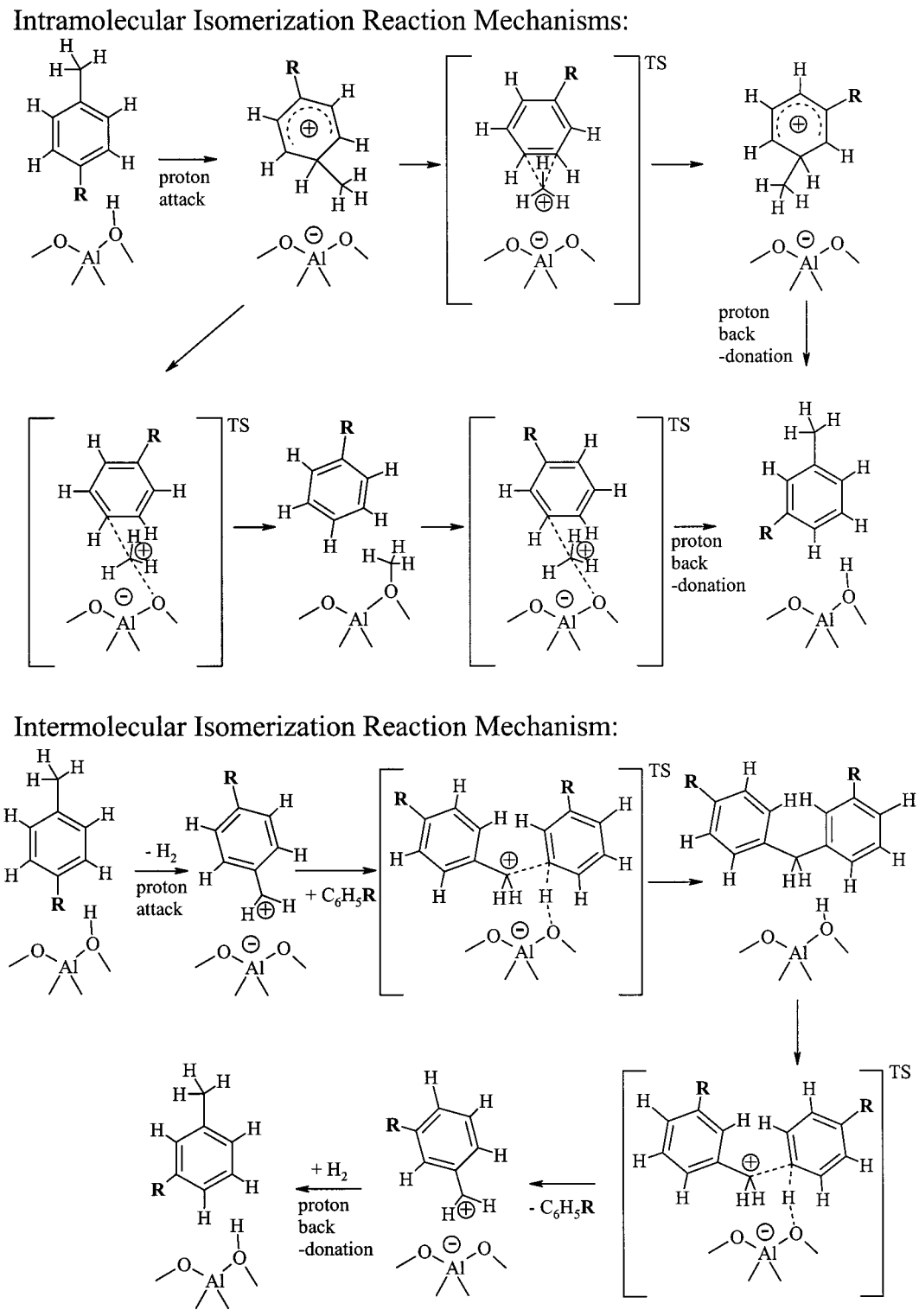

a The geometries between squared brackets are transition states.[16]

of xylene isomers catalyzed by acidic zeolites. In this study, the different reaction pathways of isomerization reactions in relation to steric constraints due to the zeolite framework on the reaction mechanism options will be investigated.

2. Methods

The periodic density functional theory (DFT) Vienna ab initio simulation package (VASP) has been used to perform all calculations.[18] This program proved its efficiency in the description of zeolites.[19−20] It has been used to perform structural studies of Brønsted acidic sites in chabazite,[19a] gmelinite,[19b,c] and mordenite.[19d] Also, studies of the adsorption of water,[20a] alkane,[20b] and benzene[21] within zeolites have been achieved. Recently, it was used to realize a study of the alkylation of toluene with methanol.[22]

The large 12-membered ring mordenite has been used for this study (see Figure 1).[23] All atoms have been allowed to relax completely within the periodic unit cell. This zeolite crystal has been extensively studied

(18) (a) Kresse, G.; Hafner, J. *Phys. Rev. B* **1993**, *48*, 13115−13126. (b) Kresse, G.; Hafner, J. *Phys. Rev. B* **1994**, *49*, 14251−14269. (c) Kresse, G.; Furthmüller, J. *Comput. Mater. Sci.* **1996**, *6*, 15−50. (d) Kresse, G.; Furthmüller, J. *Phys. Rev. B* **1996**, *54*, 11169−11186.

using VASP.[19d] Furthermore, Vos et al.[22] recently gave a complete analysis of a reaction catalyzed by acidic mordenite. We have used a similar mordenite unit cell in this study: the Si/Al ratio is 23, and the dimensions of the unit cell are $a = 13.648$ Å, $b = 13.672$ Å, $c = 15.105$, $\alpha = 96.792°$, $\beta = 90.003°$, and $\gamma = 90.022°$. The acidic mordenite unit cell is composed of 146 atoms.

Using VASP the energy is obtained by solving the Kohn−Sham equation with the Perdew−Zunger exchange-correlation functional.[24] The results are corrected for nonlocality within the generalized gradient approximation (GGA) with the Perdew−Wang 91 functional.[25,26] VASP uses plane-waves basis sets and pseudopotentials:[27] these result in a decrease of computational costs. A cutoff of 300 eV and a Brillouin zone sampling restricted to the G-point have been used. A quasi-Newton forces minimization algorithm has been used for all geometries. Convergence was assumed to be reached when forces were below 0.05 eV/Å.

The transition-state (TS) search method in VASP is the nudged elastic band (NEB) method.[28] This method also allows for the exploration of the potential energy surface for other situations other than transition states. Several geometries of the system are defined along the investigated pathway (viz., diffusion, rotation, breaking and formation of chemical bonds, etc.). These geometries or images are optimized but only allowed to move in the direction perpendicular to the current hypertangent defined by the normal vector between the neighboring images. The different images or geometries of the system are therefore connected by a nudged elastic band which induces extra forces on the geometries of system to maintain the images along the pre-established reaction pathway. We employed up to eight images connected by the elastic band to analyze transition states or other mechanisms. In the case of transition states, when forces of the images of the atoms were below 0.08 eV/Å, the maximum energy geometry was extracted, and the forces of this system were optimized separately below 0.05 eV/Å. Artificial forces which are introduced by the elastic band are removed from the atoms in this way. The NEB method has been successfully applied to the analysis of CH_x chemisorption and reaction on a ruthenium surface[29] and to the alkylation reaction of toluene within acidic mordenite.[22]

To allow comparison with experimental data, interaction energies have been corrected for the van der Waals energy dispersion contribution.[21,22] It is well-known that DFT methods within the GGA approach do not properly describe the dispersion energy contribution.2828 Pelmenschikov et al.[30d] have shown, using DFT and MP2 calculations to decompose the interaction energy, that the dispersion contribution is of the order of ˜25 kJ/mol for an aromatic species adsorbed on a neutral clay surface. The Coulombic contribution was less than half of this value. Until now no calculations of large periodic zeolite systems at the MP2 level have been reported. Demuth et al.[21] and Vos et al.[22] proposed that the dispersion contribution of aromatics physisorbed within zeolite be estimated using an empirical 12-6 Lennard-Jones potential. We used the parameters defined by Deka et al.[31] for the description of aromatics within full silicon zeolites. As parameters for the repulsion and dispersion contributions were optimized together to respect the well depth and equilibrium position r_0, they cannot be used independently, even if estimates of the repulsion contribution to the force field are not fully reliable.[32] However, the repulsion contribution is already taken into account in the chemical quantum energy calculation; only the attractive contribution needs to be considered. Therefore, we used the following relation to compute the van der Waals energy:

$$E_{\mathrm{vdW}}(r_{\mathrm{in}}) = \sum (A_{\mathrm{ij}}/r_{\mathrm{ij}}^{12} - B_{\mathrm{ij}}/r_{\mathrm{ij}}^{6}) \qquad (1)$$

The summation runs over the zeolitic atoms i and the aromatic atoms j. r_{in} corresponds to an inner cutoff below which the pair energy is not computed. The van der Waals energy is checked for r_{in} between 2 and 6 Å with a step $\Delta r_{\mathrm{in}} = 0.02$ Å. The selected van der Waals energy correction is the one yielding the lowest value as a function of r_{in}. The zeolitic host is assumed to be a completely siliceous host for this estimation. Aluminum atoms are replaced with silicon, and acidic protons are removed. Periodic conditions are applied on the unit cell that is made up of the aromatic species and the zeolite host. An external cutoff of half the dimension of the unit cell limits the summation on the pairs ij. The zeolite framework is expanded up to $2 \times 2 \times 2$ unit cells around one of the aromatic species. The volume of the mordenite supercell is 27.296 Å$^3 \times 27.344$ Å$^3 \times 30.204$ Å^3. In a classical dynamic simulation of benzene and toluene within Y zeolite pores, Klein et al.[33] decomposed the guest−host energy. They showed that the van der Waals contribution remains almost constant along the minimum energy pathway and that the electrostatic contributions, mainly Coulombic, could better explain the preferred adsorption site of aromatic species in zeolites. The importance of this electrostatic interaction is enhanced when acidic sites are present. Furthermore, in the case of hydrocarbon molecule reactions within acidic zeolite, it is well understood that transition states are of ionic nature, increasing the weight of electrostatic contribution in the identification of the structures.[1−4,10] Demuth et al.[21] show in their periodic DFT calculations study of benzene adsorption within mordenite that GGA PW91 calculations with VASP were able to give an accurate description of the non-van der Waals properties of the system.

Since the pioneering work of Haag et al.,[34] it is well established that for zeolitic catalyzed reactions the apparent activation energy is related to the adsorption energy. In the case of a monomolecular reaction, one expresses the apparent activation energy as:

$$^{\mathrm{app}}E_{\mathrm{act}} = E_{\mathrm{act}} + (1 - \Theta)\, E_{\mathrm{ads}} \qquad (2)$$

where E_{act} is the activation energy (or intrinsic activation energy), Θ the coverage of the reactant on the catalytically active site, and E_{ads} the adsorption energy of the reactant on the active site. The apparent activation energy expression is demonstrated to be rigorously correct in cases where Θ can be described by Langmuir adsorption and

(19) (a) Jeanvoine, Y.; Àngyàn, J.; Kresse, G.; Hafner, J. *J. Phys. Chem. B* **1998**, *102*, 5573−5580. (b) Benco, L.; Demuth, T.; Hafner, J.; Hutschka, F. *J. Chem. Phys.* **1999**, *111*, 7537−7545. (c) Benco, L.; Demuth, T.; Hafner, J.; Hutschka, F. *Chem. Phys. Lett.* **2000**, *324*, 373−380. (d) Demuth, T.; Hafner, J.; Benco, L.; Toulhoat, H. *J. Phys. Chem. B* **2000**, *104*, 4593−4607.

(20) (a) Jeanvoine, Y.; Àngyàn, J.; Kresse, G.; Hafner, J. *J. Phys. Chem. B* **1998**, *102*, 7307−7310. (b) Benco, L.; Demuth, T.; Hafner, J.; Hutschka, F.; Toulhoat, H. *J. Chem. Phys.* **2001**, *114*, 6327−6334.

(21) Demuth, T.; Benco, L.; Hafner, J.; Toulhoat, H.; Hutschka, F. *J. Chem. Phys* **2001**, *114*, 3703−3712.

(22) Vos, A. M.; Rozanska, X.; Schoonheydt, R. A.; Van Santen, R. A.; Hutschka, H.; Hafner, J. *J. Am. Chem. Soc.* **2001**, *123*, 2799−2809.

(23) (a) Barrer, R. M.; White, E. A. D. *J. Chem. Soc.* **1952**, *2*, 1561−1571. (b) Meier, W. M. *Z. Kristallogr.* **1961**, *115*, 439−450. (c) Rouse, R. C.; Peacor, D. R. *Am. Miner.* **1994**, *79*, 175−184.

(24) Perdew, J. P.; Zunger, A. *Phys. Rev. B* **1981**, *23*, 5048−5079.

(25) (a) Perdew, J. P.; Chevary, J. A.; Voksko, S. H.; Jackson, K. A.; Pedersen, M. R.; Singh, D. J.; Fiolhais, C. *Phys. Rev. B* **1992**, *46*, 6671−6687. (b) Perdew, J. P.; Burke, K.; Wang, Y. *Phys. Rev. B* **1996**, *54*, 16533−16539. (c) Perdew, J. P.; Burke, K.; Ernzerhof, M. *Phys. Rev. Lett.* **1996**, *77*, 3865−3868.

(26) In ref 25b and c, Perdew et al. gave a description of the PBE functional that corrects some problems of the PW91 functional. PBE functional yields essentially the same energetic results than the PW91 functional without presenting the identified problems. When the study described in ref 22 was performed, only the PW91 functional was available in VASP. To allow a direct comparison with the data in ref 22, we decided to use the same functional.

(27) Kresse, G.; Hafner, J. *J. Phys. Condens. Matter.* **1994**, *6*, 8245−8257.

(28) Mills, G.; Jónsson, H.; Schenter, G. K. *Surf. Sci.* **1995**, *324*, 305−337.

(29) (a) Ciobica, I. M.; Fréchard, F.; Van Santen, R. A.; Kleyn, A. W.; Hafner, J. *Chem. Phys. Lett.* **1999**, *311*, 185−192. (b) Ciobica, I. M.; Fréchard, F.; Van Santen, R. A.; Kleyn, A. W.; Hafner, J. *J. Phys. Chem. B* **2000**, *104*, 3364−3369.

(30) (a) Kristyan, S.; Pulay, P. *Chem. Phys. Lett.* **1994**, *229*, 175−180. (b) Sauer J.; Ugliengo, P.; Garrone, E.; Saunders: V. R. *Chem. Rev.* **1994**, *94*, 2095−2160. (c) Lein, M.; Dobson, J. F.; Gross, E. K. U. *J. Comput. Chem.* **1999**, *20*, 12−22. (d) Pelmenschikov, A.; Leszczynski, J. *J. Phys. Chem. B* **1999**, *103*, 6886−6890.

(31) (a) Deka, R. C.; Vetrivel, R. *J. Catal.* **1998**, *174*, 88−97. (b) Deka, R. C.; Vetrivel, R.; Miyamoto, A. *Topics Catal.* **1999**, *9*, 225−234.

(32) Ruthven, D. M. *Ind. Eng. Chem. Res.* **2000**, *39*, 2127−2131.

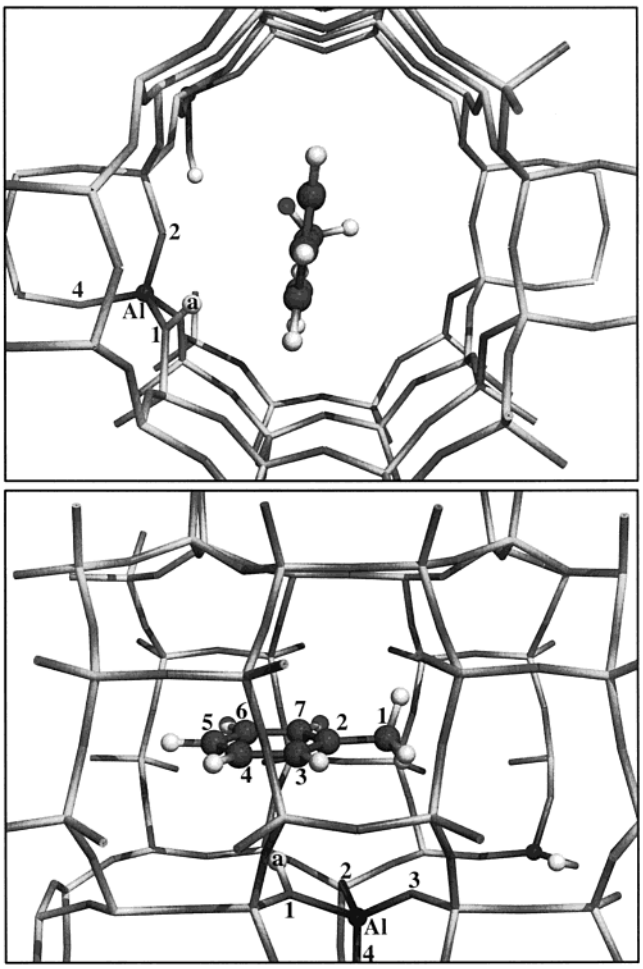

Figure 2. Geometry of toluene adsorbed on acidic site of H-MOR as obtained from the periodic calculations. The labels used in this Figure will be the same for all others geometries: these constitute the reference. In the case of xylene isomers the extra methyl group carbon atom will be C_8.

competitive product or intermediate adsorption can be ignored.[35] From eq 2 it appears clearly that a good estimate of E_{ads} is required. The van der Waals energy contribution of the periodic geometry has therefore been estimated using eq 1.

3. Results

3.1. Toluene Isomerization. In this part toluene isomerization reactions catalyzed by acidic mordenite will be investigated. The monomolecular isomerization reaction of toluene is believed to occur following two reaction pathways.[15,16,36] It can be achieved through a methyl shift reaction step (shift mechanism) or via benzene and a methoxy intermediate (disproportionation mechanism) (see Scheme 1).

Both reaction pathways are initiated when toluene adsorbs on a proton site within a mordenite micropore. In our calculations it is found that toluene adopts an η^2(CC) adsorption mode with respect to the acidic site (**Ads_tol**) (see Figures 2 and 3). A toluene C═C bond interacts with the acidic proton (H_aC_3 = 2.64 Å and H_aC_4 = 2.74 Å) (see Table 1). The toluene methyl group is oriented in the 12-membered ring channel direction. The adsorption energy of toluene is −31 kJ/mol in the absence

Table 1. Selected Bond Lengths (Å), Angles (degrees) and Dihedral Angles (degrees) of Adsorbed Complex, Transient Species and Transition State for the Isomerization Reaction of Toluene Catalyzed by Acidic Mordenite as Obtained from the Periodic Calculations[a]

Ads_tol		**Pro_tol**		**C_tol2**		**TS_shift_tol1**	
AlO_1	1.9	AlO_1	1.78	AlO_1	1.73	AlO_1	1.73
AlO_2	1.69	AlO_2	1.72	AlO_2	1.73	AlO_2	1.72
AlO_3	1.7	AlO_3	1.72	AlO_3	1.74	AlO_3	1.74
AlO_4	1.69	AlO_4	1.71	AlO_4	1.71	AlO_4	1.71
AlO_1Si_1	135.9	AlO_1Si_1	135.1	AlO_1Si_1	147.3	AlO_1Si_1	143.7
H_aO_1	0.99	H_aO_1	1.79	H_aO_1	2.57	H_aO_1	2.48
H_aC_3	2.64	H_aC_2	1.19	H_aC_2	1.1	C_1C_2	1.89
H_aC_4	2.74	C_1C_2	1.53	C_1C_2	1.63	C_1C_3	1.85
C_1C_2	1.5	$C_1C_2C_3C_7$	144.1	C_1O_3	2.96	C_1O_3	3.06
$O_1H_aC_3$	132.5	$H_aC_2C_3C_7$	−103.5	H_3O_2	2.92	C_1O_2	3.02
$O_1H_aC_4$	144.2			$C_1C_2C_3C_7$	108.3	H_3O_2	2.8
AlO_1H_a	107.2			$H_aC_2C_3C_7$	−140.2	$C_1C_2C_3$	66
						$C_1C_3C_2$	69
						$C_1C_2C_3C_4$	99.8

[a] The labels used in this table are defined in Figure 2 for the atoms and in Figure 3 for the configurations.

Table 2. Selected Bond Lengths (Å), Angles (degrees), and Dihedral Angles (degrees) of Transient Species and Transition State for the Isomerization Reaction of Toluene Catalyzed by Acidic Mordenite as Obtained from the Periodic Calculations[a]

C_tol1		**TS_shift_tol2**		**σ-complex**	
AlO_1	1.73	AlO_1	1.73	AlO_1	1.71
AlO_2	1.73	AlO_2	1.72	AlO_2	1.84
AlO_3	1.75	AlO_3	1.73	AlO_3	1.73
AlO_4	1.71	AlO_4	1.73	AlO_4	1.7
AlO_1Si_1	146.3	AlO_1Si_1	143	AlO_1Si_1	144.7
H_aO_1	2.74	C_1C_2	1.91	AlO_2Si_2	130.7
H_aC_2	1.12	C_1C_7	1.91	AlO_2C_3	107.3
C_1C_2	1.56	C_7O_2	3.75	O_2C_3	1.8
$C_1C_2C_3C_7$	132	C_2O_3	4.38	H_aC_2	1.1
$H_aC_2C_3C_7$	−115.1	$C_1C_2C_7$	68	H_3C_3	1.09
		$C_1C_7C_2$	68.2	C_1C_2	1.56
		$C_1C_2C_7C_6$	99.4	$O_2C_3C_2C_7$	100
				$C_1C_2C_3C_4$	99.5

[a] The labels used in this table are defined in Figure 2 for the atoms and in Figure 3 for the configurations.

of the van der Waals energy correction. This value is lowm but this is not surprising as DFT methods do not describe the dispersion contributions correctly.[20b,21,22,30] It is well-known that the adsorption of aromatics within zeolite is dominated by van der Waals contributions.[31,37]

Toluene is protonated before it isomerizes. It was shown before by zeolite small cluster appoach theoretical studies that the protonated state is a transient state.[8,12,16,22] DFT periodic calculations gives us the opportunity to check the zeolite framework electrostatic effect on the protonation step. The nudged elastic band method allows an analysis of the protonation. Eight images are used to investigate toluene protonation on the C_α aromatic ring position with respect to the methyl group. An increase of the energy for the different images along the elastic band is observed as a function of the distance O_1H_a. Force minimization of an intermediate geometry between adsorbed toluene and protonated toluene leads to a stable zero-forces (forces below 0.05 eV/Å) geometry (**Pro_tol)** (see Figure 3). For this transient state the toluene methyl group and the hydrogen atom H_a did not reach their equilibrium positions as expected for a Wheland complex geometry. Force minimization of protonated toluene gives **C_tol1** geometry (see Figure 3). The dihedral angle $C_1C_2C_3C_7$ is 144.1° and 132° for **Pro_tol** and **C_tol1** respectively (see Tables 1 and 2). For $H_aC_2C_3C_7$

(33) Klein, H.; Kirschhoch, C.; Fuess, H. *J. Phys. Chem.* **1994**, *98*, 12345−12360.

(34) Haag W. O. *Zeolites and Related Microporous Materials, State of the Art 1994*, Weitkamp, H. G, Karge, H., Pfeifer, H., Hölderich, W., Eds.; Elsevier Science: Amsterdam, 1994; pp 1375−1394.

(35) Van Santen, R. A.; Niemanstverdriet, J. W. *Chemical Kinetics and Catalysis*; Plenum Press: New York, 1995.

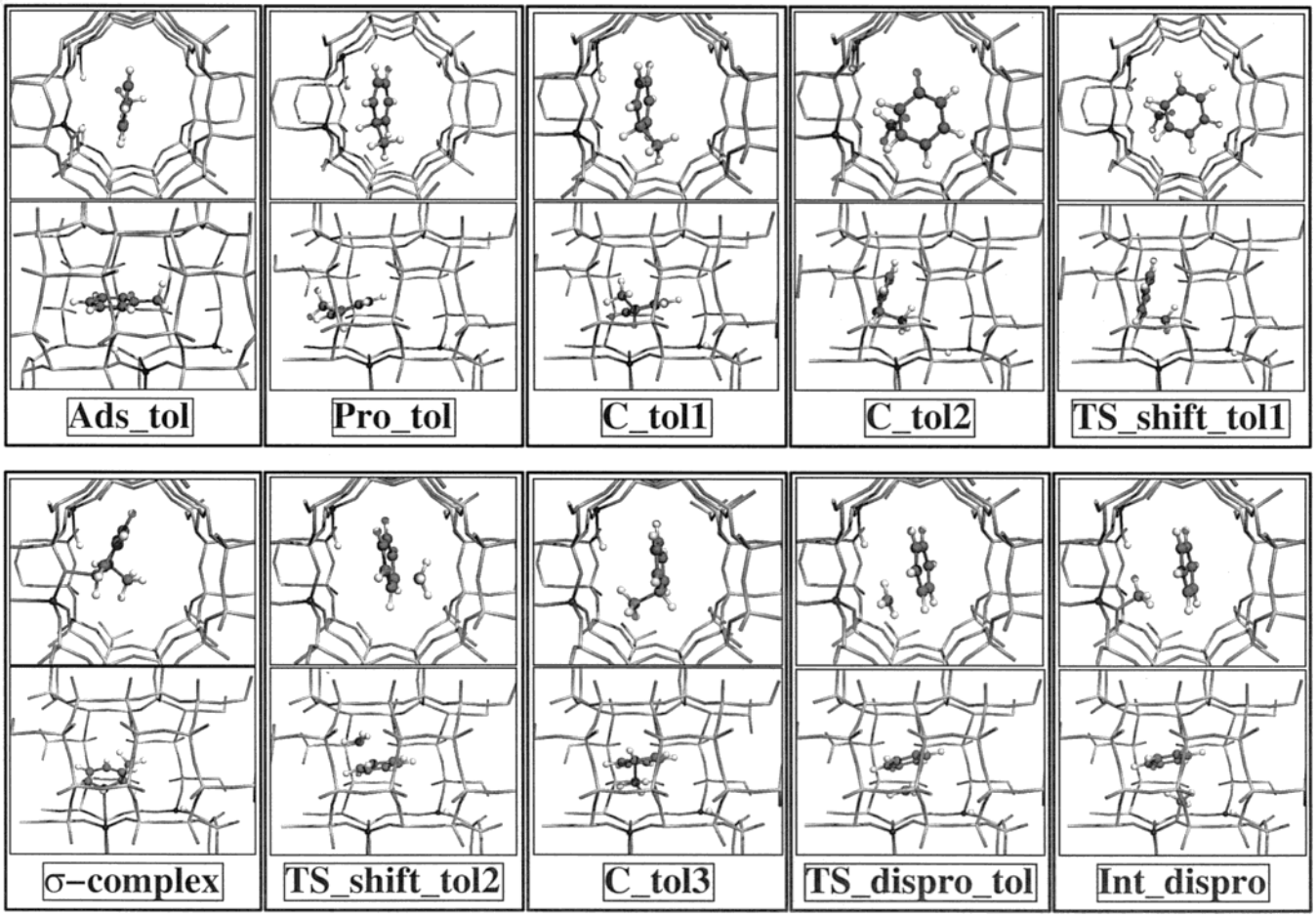

Figure 3. Front and side views of the intermediates and transition states for the isomerization reaction pathways of toluene catalyzed by acidic mordenite as obtained from the periodic calculations. All geometries have been gathered in this single scheme.

the angle is −103.5° and −115.1° for **Pro_tol** and **C_tol1**, respectively. The energy level of **Prot_tol** is +108 kJ/mol with respect to adsorbed toluene. In the case of **C_tol1** it is +111 kJ/mol. It clearly appears that toluene protonation does not correspond to a transition state but rather to an inflection point on the reaction pathway toward isomerization.

We will consider first the shift isomerization reaction. We defined a reaction pathway that corresponds to a mechanism as observed in the case of cluster approach results (see Figure 4).[16b] Another protonated toluene geometry is defined (see **C_tol2** in Figure 3). This intermediate corresponds to the geometry that is adopted by toluene before the methyl shift reaction step occurs. The energy level of **C_tol2** is +135 kJ/mol with respect to adsorbed toluene.

The existence of the σ-bonded species or a phenoxy intermediate has been probed (see **σ-complex** in Figure 3 and Table 2). The alkoxy species resulting from a proton attack are observed to be more stable than the physisorbed state in the case of olefins.[11] In the case of toluene the phenoxy intermediate is +150 kJ/mol higher in energy than the adsorbed state. This energy level is similar to that obtained using the cluster approach method (+150 vs +152 kJ/mol).[16b] This intermediate is, however, less stable than protonated toluene as in the case of the **C_tol1** and **C_tol2** geometries. From the **C_tol2** geometry, an eight-images NEB system was defined to localize the shift isomerization maximum energy. The obtained top energy geometry has been optimized using a quasi-Newton forces minimization algorithm afterward. This procedure leads to the transition state **TS_shift_tol1** (maximum in energy and zero forces) of the shift isomerization reaction (see Figure 3 and Table 1). In this transition state the shifting methyl group occupies an intermediate localization between the toluene aromatic ring carbon atoms C_2 and C_3 (C_1C_2 = 1.89 Å, C_1C_3 = 1.85 Å, $C_1C_2C_3$ = 66°, and $C_1C_3C_2$ = 69°). The plane that is defined by atoms C_1, C_2, and C_3 is almost perpendicular to the toluene aromatic ring ($C_1C_2C_3C_4$ = 99.8°). Furthermore, the shifting methyl group is located at equal distances from the Brønsted site oxygen atoms O_2 and O_3 (C_1O_2 = 3.02 Å and C_1O_3 = 3.06 Å). The activation energy of this isomerization reaction with respect to **Ads_tol** is +179 kJ/mol. **Pro_tol**, **C_tol1** and **C_tol2** do not correspond to minima but rather to transient situations that show zero-forces.

The shift isomerization reaction path without further reorientation of protonated toluene was followed from the **C_tol1** geometry (see Figure 3 and Table 2). The transition-state geometry **TS_shift_tol2** was obtained (see Figure 3). The aromatic ring interacts with the Brønsted site oxygen atoms through a C=C bond (C_7O_2 = 3.75 Å and C_2O_3 = 4.38 Å) in this transition state. The position of the shifting methyl group with respect to the aromatic ring is very similar to the position in the case of **TS_shift_tol1** ($C_1C_2 = C_1C_7$ = 1.91 Å and $C_1C_2C_3C_7$ = 99.4°). Interestingly, the activation energy obtained with this reaction pathway (**TS_shift_tol2**) is equal to the previous one (**TS_shift_tol1**) (E_{act} = +179 kJ/mol).[38]

Next, we consider the isomerization reaction path that proceeds via a methyl alkoxy and benzene intermediate. This intermediate is obtained after the disproportionation reaction of toluene. A second disproportionation reaction step generates

(36) (a) Cortes, A.; Corma, A. *J. Catal.* **1978**, *51*, 338−344. (b) Beschmann, K.; Riekert, L. *J. Catal.* **1993**, *141*, 548−565.

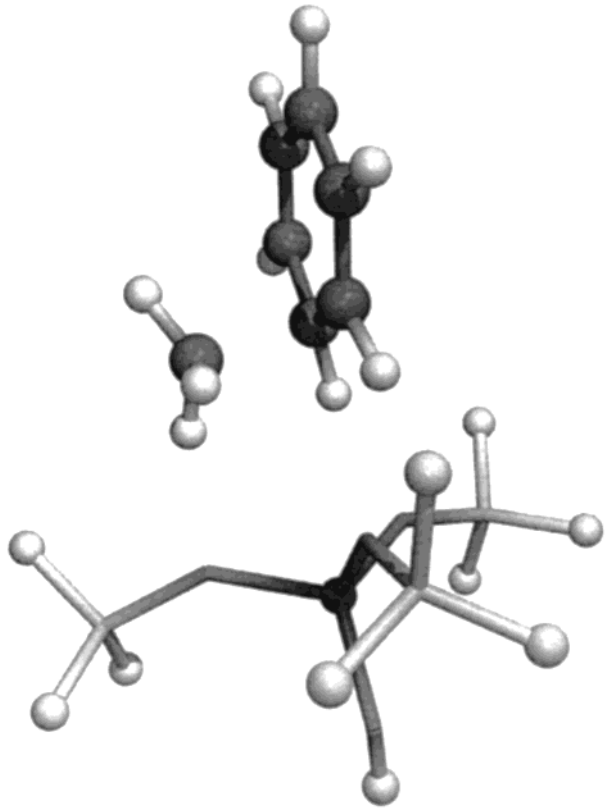

Figure 4. Transition-state geometry of the toluene shift isomerization reaction as obtained using a cluster approach method.[16b]

Table 3. Selected Bond Lengths (Å), Angles (degrees), and Dihedral Angles (degrees) of Transient Species, Transition State, and Intermediate for the Isomerization Reaction of Toluene Catalyzed by Acidic Mordenite as Obtained from the Periodic Calculations

C_tol3		**TS_dispro_tol**		**Int_dispro_tol**	
AlO_1	1.73	AlO_1	1.72	AlO_1	1.69
AlO_2	1.72	AlO_2	1.71	AlO_2	1.69
AlO_3	1.74	AlO_3	1.8	AlO_3	1.92
AlO_4	1.72	AlO_4	1.7	AlO_4	1.7
AlO_1Si_1	142.7	AlO_1Si_1	145.7	AlO_1Si_1	149.1
C_1C_2	1.61	C_1C_2	2.18	C_1C_2	3.22
H_aC_2	1.1	C_1O_3	2.12	C_1O_3	1.49
C_1O_1	3.31	O_3C_2	4.3	O_3C_2	4.59
C_1O_3	3.06	AlO_3Si_3	138.4	AlO_3Si_3	133.5
O_3C_2	4.58	$O_3C_1C_2$	177		
$C_1C_2C_3C_4$	105.5				
$H_aC_2C_3C_4$	−143				

[a] The labels used in this table are defined in Figure 2 for the atoms and in Figure 3 for the configurations.

isomerized toluene. Once protonation of toluene has occurred, the transient charged species reorients itself to present its methyl group to a Brønsted site oxygen atom (see **C_tol3** in Figure 3 and Table 3). This configuration (+130 kJ/mol above **Ads_tol**. **C_tol3**) is used as a starting configuration to define an eight-images NEB that connects this geometry to both the methoxy group and benzene. These calculations allow for the identification of the disproportionation transition state **TS_dispro_tol** (see Figure 3 and Table 3). This transition state can be described as a methylenium carbocation that is sandwiched between benzene and the deprotonated Brønsted site. The bonds between the methyl group carbon atom and the aromatic ring carbon atom C_2 and the Brønsted site oxygen atom O_3 are not yet formed (C_1C_2 = 2.18 Å and C_1O_3 = 2.12 Å) (see Table 3). The activation energy of this reaction step is +182 kJ/mol with respect to **Ads_tol**. This transition state leads to the formation of methoxy and benzene (see **Int_dispro** in Figure 3). This intermediate is not very stable. It is +87 kJ/mol above **Ads_tol**. Benzene can desorb from methoxy, change its orientation and even diffuse away. The **TS_dispro_tol** reverse-mechanism restores a toluene molecule (E_{act} = +95 kJ/mol).

Table 4. Selected Bond Lengths (Å), Angles (degrees), and Dihedral Angles (degrees) of Adsorbed Complex and Transient Species for the Isomerization Reaction of *para*-Xylene Catalyzed within Acidic Mordenite as Obtained from the Periodic Calculations[a]

Ads_pxy		**C_pxy**	
AlO_1	1.9	AlO_1	1.72
AlO_2	1.69	AlO_2	1.72
AlO_3	1.7	AlO_3	1.74
AlO_4	1.69	AlO_4	1.73
AlO_1Si_1	135.9	AlO_1Si_1	142.9
O_1H_a	0.99	H_aC_2	1.12
H_aC_3	2.61	H_aC_1	3.32
H_aC_4	2.72	H_aO_3	3.06
C_1C_2	1.5	C_1C_2	1.57
$O_1H_aC_3$	134.3	$C_1C_2C_3C_4$	127.4
$O_1H_aC_4$	145.7	$H_aC_2C_3C_4$	−119.1

[a] The labels used in this table are defined in Figure 2 for the atoms and in Figure 5 for the configurations.

Table 5. Selected Bond Lengths (Å), Angles (degrees) and Dihedral Angles (degrees) of Adsorbed Complex, Transient Species and Transition State for the Isomerization Reaction of *meta*-Xylene Catalyzed by Acidic Mordenite as Obtained from the Periodic Calculations

Ads_mxy		**C_mxy**		**TS_shift_mp_xy2**	
AlO_1	1.9	AlO_1	1.73	AlO_1	1.73
AlO_2	1.68	AlO_2	1.72	AlO_2	1.72
AlO_3	1.7	AlO_3	1.74	AlO_3	1.73
AlO_4	169	AlO_4	1.72	AlO_4	1.73
AlO_1Si_1	132.4	AlO_1Si_1	142.5	AlO_1Si_1	143.1
O_1H_a	0.99	H_aC_2	1.11	C_1C_2	1.9
H_aC_3	2.48	H_aO_1	3.36	C_1C_3	1.93
H_aC_4	2.84	H_aO_3	3.14	O_1C_2	4.49
C_1C_2	1.5	C_1C_2	1.58	O_2C_2	4.15
$O_1H_aC_3$	148.1	$C_1C_2C_3C_4$	123.2	O_3C_2	4.39
$O_1H_aC_4$	142.3	$H_aC_2C_3C_4$	−124.4	$C_1C_2C_3$	69.4
				$C_1C_3C_2$	66.9
				$C_1C_2C_3C_4$	99

[a] The labels used in this table are defined in Figure 2 for the atoms and in Figure 5 for the configurations.

3.2. Xylene Isomerization. We will now extend the calculations to the study of *para*-, *meta*-, and *ortho*-xylenes isomerization reactions catalyzed by acidic mordenite.

The adsorption configuration mode for the *para*-xylene isomer is η^2(CC) (H_aC_3 = 2.61 Å and H_aC_4 = 2.72 Å) (see Table 4) with both methyl groups oriented along the large 12-membered ring channel (see **Ads_pxy** in Figure 5). The adsorption energy is −37 kJ/mol. The preferred adsorption geometries allow less interactions between the xylene methyl groups and the zeolite walls (see **Ads_mxy** and **Ads_oxy** in Figure 5). The xylene molecule adopts a η^2(CC) adsorption mode (for adsorbed *meta*-xylene (**Ads_mxy**), H_aC_3 = 2.48 Å and H_aC_4 = 2.84 Å and for adsorbed *ortho*-xylene (**Ads_oxy**), H_aC_3 = 2.41 Å and H_aC_4 = 2.44 Å) (see Tables 5 and 6). The adsorption energies for *meta*-xylene and *ortho*-xylene are −30 kJ/mol and −32 kJ/mol, respectively. **Ads_oxy** and **Ads_mxy** are less stable than **Ads_pxy**. This is mainly explained by the geometries of the xylene molecules and by the curvature of the zeolite wall close to the acidic site. Interaction with an acidic proton located on the oxygen atom O_2 gives similar differences of adsorption energy for all three xylene molecules. The adsorption energies

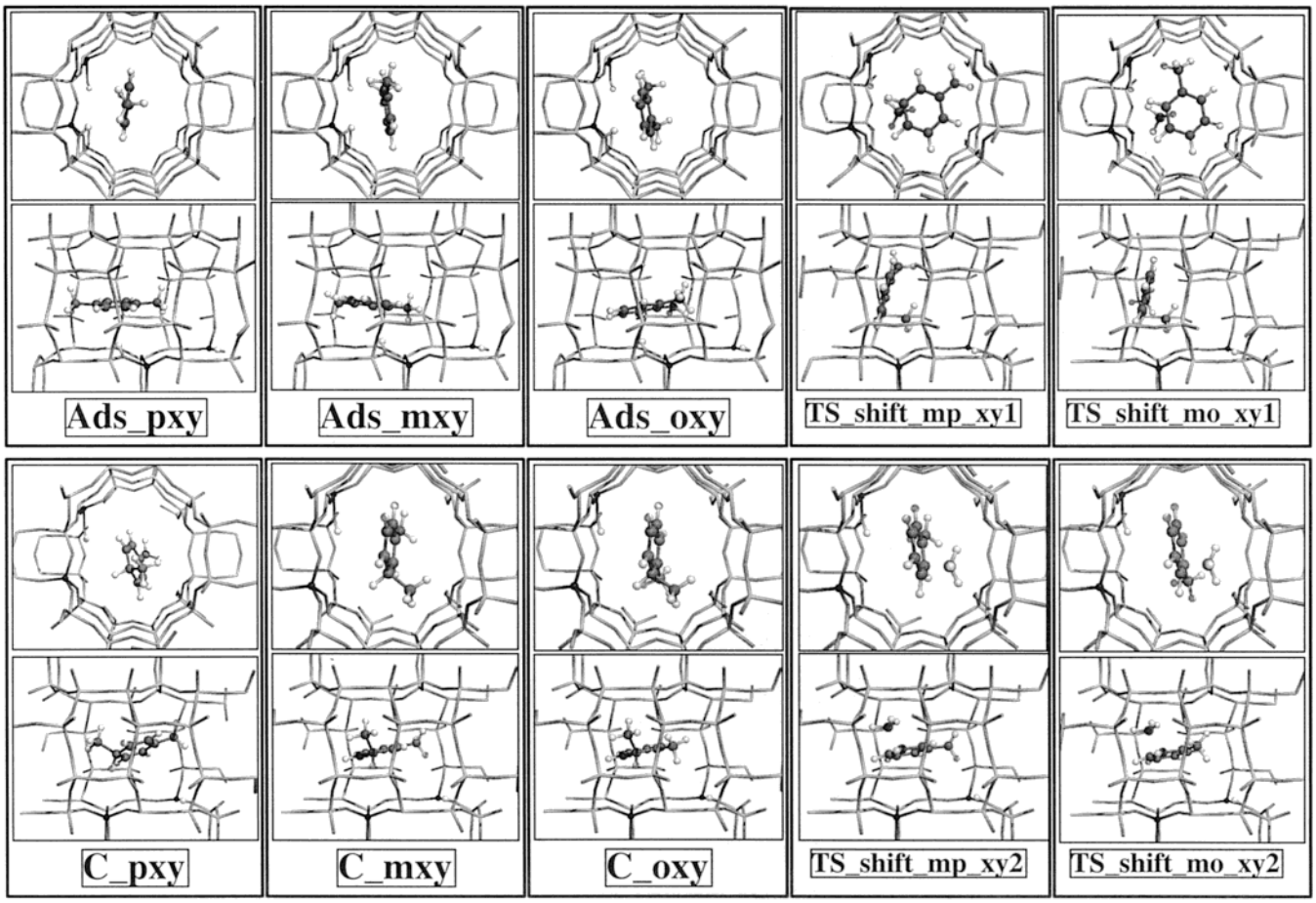

Figure 5. Front and side views of the intermediates and transition states for the shift isomerization reaction pathways of xylene molecules catalyzed by acidic mordenite as obtained from the periodic calculations.

Table 6. Selected Bond Lengths (Å), Angles (degrees), and Dihedral Angles (degrees) of Adsorbed Complex, Transient Species and Transition State for the Isomerization Reaction of *ortho*-Xylene Catalyzed by Acidic Mordenite as Obtained from the Periodic Calculations

Ads_oxy		**C_oxy**		**TS_shift_mo_xy2**	
AlO_1	1.9	AlO_1	1.73	AlO_1	1.73
AlO_2	1.69	AlO_2	1.72	AlO_2	1.72
AlO_3	1.7	AlO_3	1.74	AlO_3	1.74
AlO_4	1.7	AlO_4	1.72	AlO_4	1.73
AlO_1Si_1	133.6	AlO_1Si_1	142.6	AlO_1Si_1	143.1
O_1H_a	0.99	H_aC_2	1.1	C_1C_2	1.94
H_aC_3	2.41	H_aC_1	3.36	C_1C_3	1.88
H_aC_4	2.44	H_aO_3	3.13	O_1C_2	4.48
C_1C_2	1.5	C_1C_2	1.58	O_2C_2	4.14
$O_1H_aC_3$	142.5	$C_1C_2C_3C_4$	123.1	O_3C_2	4.36
$O_1H_aC_4$	154.6	$H_aC_2C_3C_4$	−124.2	$C_1C_2C_3$	65.9
				$C_1C_3C_2$	70.2
				$C_1C_2C_3C_4$	100.6

[a] The labels used in this table are defined in Figure 2 for the atoms and in Figure 5 for the configurations.

for *para*-xylene, *meta*-xylene, and *ortho*-xylene on this acidic site are −36, −23, and −30 kJ/mol, respectively. As this other adsorption site does not result in more stable configurations, it was not considered further. Xylene molecules are sufficiently small compared with the dimension of mordenite channels to be accommodated within the micropore structure. The differences between adsorption energies for the three isomers result from the local topology of the Brønsted site.

The protonation reaction steps show the same trend as in the case of toluene. The protonation reaction steps correspond to inflection points on the reaction pathways for all isomers. Only the details for the protonated xylene molecules are reported here. Protonation of *ortho*-xylene is endothermic with respect to its π-adsorption mode with a value of +88 kJ/mol above **Ads_oxy** (see **C_oxy** in Figure 5). Protonated *meta*- (**C_mxy**) and *para*-xylene (**C_pxy**) have comparable energies. The protonated species energies are +95 and +98 kJ/mol respectively with respect to their correspondent ground adsorption states.

Shift isomerization reactions and the isomerization reaction via a disproportionation reaction step of xylene isomers have been considered as was done for toluene. Two different shift isomerization reaction pathways have been considered.

Concerning *ortho*-xylene the shift isomerization reaction leads to the formation of *meta*-xylene. The first transition state relates to a mechanism similar to that obtained via cluster studies (see **TS_shift_mo_xy1** in Figure 5). One can see that the nonparticipating methyl group is in relatively close proximity to the zeolite atoms in this transition state. The geometry of the TS shows asymmetry (C_1C_2 = 1.90 Å, C_1C_3 = 1.83 Å, H_3O_1 = 2.49 Å and H_aO_2 = 2.82 Å) (see Table 7). The activation energy of this reaction step is +184 kJ/mol with respect to adsorbed *ortho*-xylene. The transition state, that follows immediately the protonation step without reorientation of the aromatic molecule, has a lower energy (E_{act} is 14 kJ/mol lower). It can be seen in Figure 5 that this reaction step allows the nonparticipating methyl group to avoid close interaction with the zeolite wall (see **TS_shift_mo_xy2** in Figure 5). The shifting methyl group in **TS_shift_mo_xy2** occupies a position that is analogous to that in **TS_shift_mo_xy1** (C_1C_2 = 1.94 Å and C_1C_3 = 1.88 Å) (see Table 6).

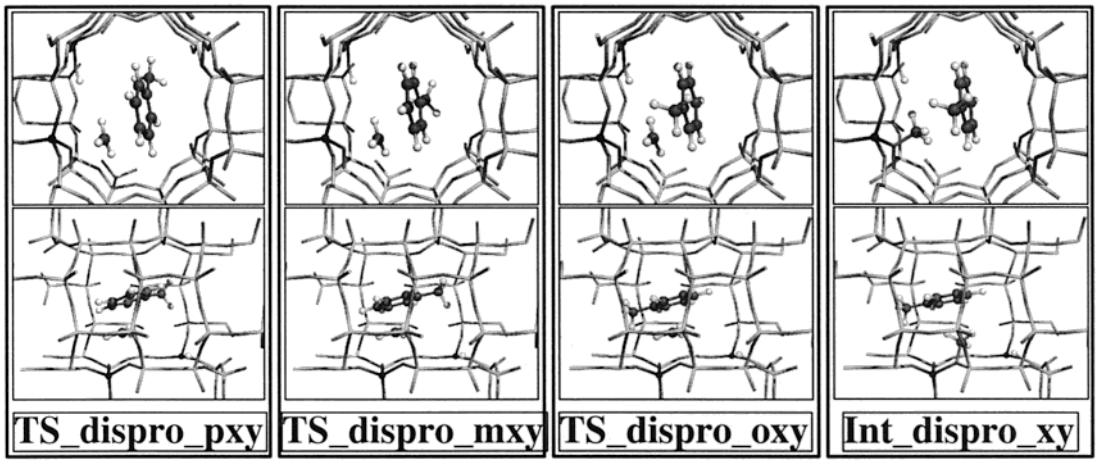

Figure 6. Front and side views of the intermediates and transition states for the isomerization reaction via disproportionation reaction pathway of xylene molecules catalyzed by acidic mordenite as obtained from the periodic calculations.

Table 7. Selected Bond Lengths (Å), Angles (degrees), and Dihedral Angles (degrees) of Transition States for the Isomerization Reaction of Xylene Isomers Catalyzed by Acidic Mordenite as Obtained from the Periodic Calculations[a]

TS_shift_mo_xy1		**TS_shift_mp_xy1**	
AlO_1	1.73	AlO_1	1.74
AlO_2	1.72	AlO_2	1.71
AlO_3	1.74	AlO_3	1.74
AlO_4	1.71	AlO_4	1.72
AlO_1Si_1	143.9	AlO_1Si_1	144.8
C_1C_2	1.9	C_1C_2	1.84
C_1C_3	1.83	C_1C_3	1.91
C_1O_3	3.03	C_1O_3	3
C_1O_1	3.52	C_1O_1	3.02
H_3O_1	2.49	H_3O_1	2.25
H_aO_2	2.82	H_aO_2	2.77
$C_1C_2C_3$	64.9	$C_1C_2C_3$	70.2
$C_1C_3C_2$	70.2	$C_1C_3C_2$	65.2
$C_1C_2C_3C_4$	99.1	$C_1C_2C_3C_4$	96.7

[a] The labels used in this table are defined in Figure 2 for the atoms and in Figure 5 for the configurations.

In the case of the *para*-xylene to *meta*-xylene transition state, analogous to that obtained via the cluster approach, steric constraints contribute even more to destabilization of the transient species than in the previous case (see **TS_shift_mp_xy1** in Figure 5). The nonparticipating methyl group is in very close interaction with the zeolite wall in this TS. This results in short distances between the aromatic ring and the Brønsted site oxygen atoms (H_3O_1 = 2.25 Å and H_aO_2 = 2.77 Å) (see Table 7). The position of the shifting methyl is also nonsymmetrical with respect to C_2 and C_3 carbon atoms but opposite with respect to **TS_shift_mo_xy1** or **TS_shift_mo_xy2** (C_1C_2 = 1.84 Å and C_1C_3 = 1.91 Å). **TS_shift_mp_xy1** shows a significant activation energy due to the steric constraints experienced by the aromatic species (E_{act} = +224 kJ/mol with respect to adsorbed *para*-xylene). The shift isomerization reaction that occurs prior to reorientation of the xylene molecule shows negligible steric interactions between the nonparticipating methyl group and the zeolite wall (see **TS_shift_mp_xy2** in Figure 5). The activation energy is 53 kJ/mol lower in comparison with **TS_shift_mp_xy1** (E_{act} = +171 kJ/mol with respect to adsorbed *para*-xylene). For **TS_shift_mp_xy2** the shifting methyl group is located at an intermediate position between C_2 and C_3 (C_1C_2 = 1.90 Å and C_1C_3 = 1.93 Å) (see Table 5).

The transition states of the isomerization reaction that proceed via the disproportionation reaction have been considered for the three xylene isomers. The position of the jumping methyl group is very similar for the different transition states. This is also the case for the position of the aromatic ring with respect to the Brønsted site oxygen atoms (see Table 8). However, the activation energy difference is around 15 kJ/mol. This difference is not due to steric constraints. As is seen in Figure 6 the nonparticipating methyl groups are not in close proximity to the zeolite wall (see **TS_dispro_pxy**, **TS_dispro_mxy** and **TS_dispro_oxy** for reactions of *para*-xylene, *meta*-xylene, and *ortho*-xylene, respectively, in Figure 6). The activation energy for **TS_dispro_oxy** is the lowest one, with E_{act} = +164 kJ/mol with respect to adsorbed *ortho*-xylene. In the case of **TS_dispro_pxy** and **TS_dispro_mxy** the activation energies are +174 and +187 kJ/mol with respect to adsorbed *para*-xylene and *meta*-xylene, respectively.

Table 8. Selected Bond Lengths (Å), Angles (degrees) and Dihedral Angles (degrees) of Intermediate and Transition States for the Isomerization Reaction of Xylene Isomers Catalyzed by Acidic Mordenite as Obtained from the Periodic Calculations[a]

TS_dispro_oxy		**TS_dispro_mxy**		**TS_dispro_pxy**		**Int_dispro_xy**	
AlO_1	1.72	AlO_1	1.71	AlO_1	1.71	AlO_1	1.69
AlO_2	1.71	AlO_2	1.71	AlO_2	1.71	AlO_2	1.69
AlO_3	1.8	AlO_3	1.8	AlO_3	1.8	AlO_3	1.92
AlO_4	1.7	AlO_4	1.71	AlO_4	1.71	AlO_4	1.7
AlO_1Si_1	145.8	AlO_1Si_1	145.8	AlO_1Si_1	145.5	AlO_1Si_1	149
C_1C_2	2.22	C_1C_2	2.19	C_1C_2	2.22	C_1C_2	3.22
C_1O_3	2.07	C_1O_3	2.12	C_1O_3	2.09	C_1O_3	1.5
O_3C_2	4.29	O_3C_2	4.31	O_3C_2	4.3	O_3C_2	4.6
AlO_3Si_3	137.5	AlO_3Si_3	137.7	AlO_3Si_3	137.3	AlO_3Si_3	133.4
$O_3C_1C_2$	177	$O_3C_1C_2$	176.7	$O_3C_1C_2$	174		

[a] The labels used in this table are defined in Figure 2 for the atoms and in Figure 6 for the configurations

Only the most stable configuration of the product of this reaction is shown (see **Int_dispro_xy** in Figure 6). **Int_dispro_xy** represents a methoxy group and a toluene molecule formed after the disproportionation reaction of *ortho*-xylene. It is +78, +86, and +76 kJ/mol with respect to adsorbed *ortho*-, *para*-, and *meta*-xylene, respectively. The configuration of the intermediate formed after the disproportionation reaction of *para*-xylene is 2 kJ/mol less stable than **Int_dispro_xy**, whereas it is 14 kJ/mol less stable in the case of *meta*-xylene.

Except for *ortho*-xylene the isomerization reactions via disproportionation mechanism show higher activation energies than the shift isomerization reactions.

4. Discussion

Toluene Isomerization. The reaction energy diagrams corresponding to the three different reaction pathways of the toluene

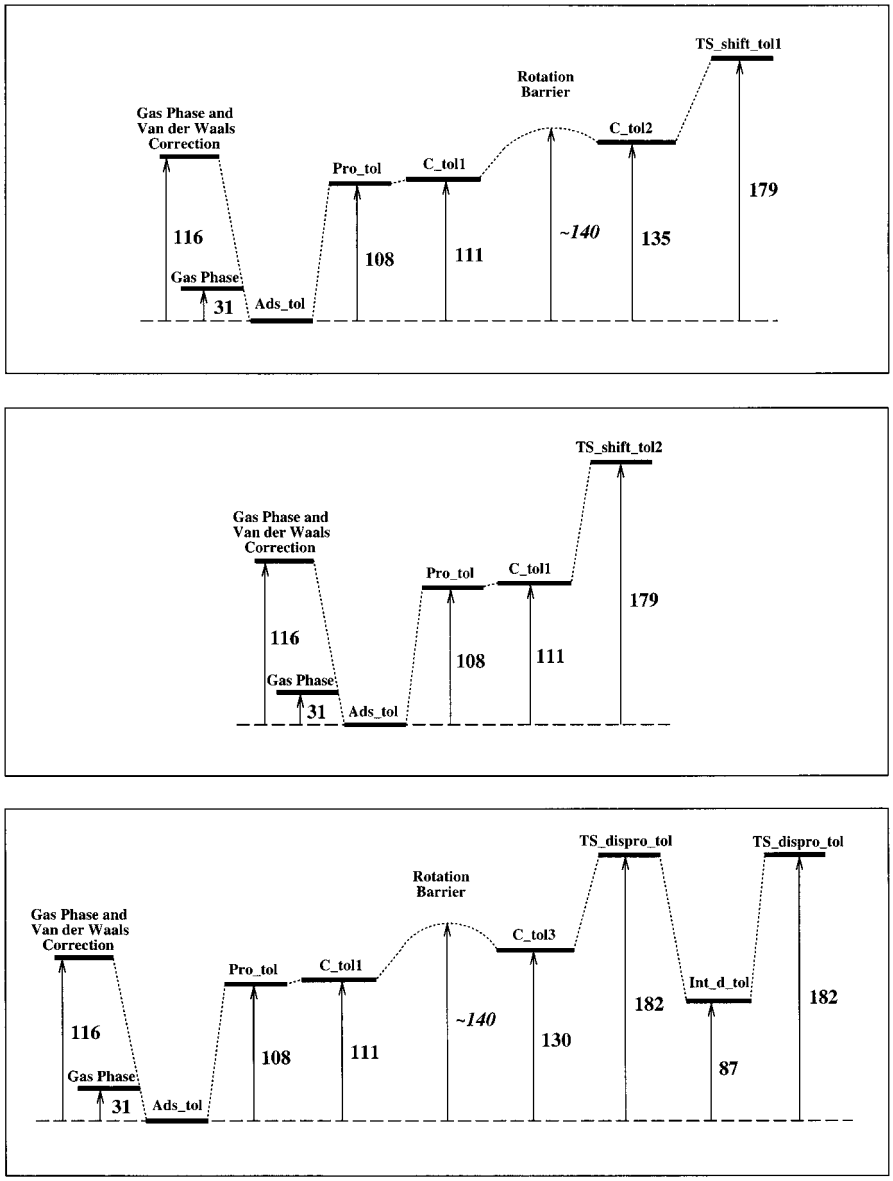

Figure 7. Reaction energy diagrams of toluene catalyzed by acidic mordenite for the shift isomerization reaction according to a mechanism similar to as obtained in cluster calculation (top), the shift isomerization reaction that occurs immediately after the protonation step (middle) and the isomerization reaction via disproportionation reaction step (bottom). All values are in kJ/mol. The labels used in this Figure are the same as in Figure 3.

isomerization reaction are depicted in Figure 7. The rotational energy barriers of the protonated species around its C_2 axis have been estimated using experimental data in this figure.[17a,39] As mentioned in the Methods section the toluene adsorption energy has been corrected for the van der Waals dispersion energy contribution. This energy contribution is estimated to be −85 kJ/mol. The corrected adsorption energy of toluene is $E_{ads} = -116$ kJ/mol, in good agreement with reported data.[31,40] The apparent activation energy for the isomerization reaction can be calculated using eq 2. It varies between around +60 to +120 kJ/mol for a coverage Θ between 0 and 0.5.

Interestingly, it appears impossible to discriminate between the two reaction pathways (see Table 9). Such results were also obtained using cluster approach calculations.[16b] This illustrates a drawback and an advantage of the cluster approach. On one hand the cluster approach method dramatically overestimates activation energies. On the other hand it conserves the relative order of activation energies, making this method suitable for qualitative comparative reactivity studies. However, small-size cluster models are unable to describe reaction pathways that proceed through mechanisms such as the **TS_shift_tol2** transition state. The shifting methenium ion is stabilized by zeolitic oxygen atoms other than those of the Brønsted site in this reaction pathway (see Figure 8). A close look at the electronic density of the Brønsted site oxygen atoms and other zeolitic oxygen atoms shows that all neighboring zeolitic atoms can play a role in the stabilization of cation nature transition state (see Figure 9).[39] This stabilization appears to occur via weak hydrogen bonds. This is in agreement with earlier observations.[42]

(37) (a) Bezuz, A. A.; Kiselev, A. G.; Loptakin, A. A.; Quang Du, P. *J. Chem. Soc., Faraday Trans. 2* **1978**, *74*, 367−379. (b) Meinander, N.; Tabisz, G. C. *J. Chem. Phys.* **1983**, *79*, 416−421. (c) Lachet, V.; Boutin, A.; Tavitian, B.; Fuchs, A. H. *Langmuir* **1999**, *15*, 8678−8685.

(38) All values have been rounded up to kJ/mol in this study.

(39) (a) Jobic, H.; Bee, M.; Renoupez, A. *Surf. Sci.* **1984**, *140*, 307−320. (b) Sato, T.; Kunimori, K.; Hayashi, S. *Phys. Chem. Chem. Phys.* **1999**, *1*, 3839−3843.

Table 9. Activation Energies of the Reactions Considered in This Study as Obtained from the DFT Periodic Calculations (at 0 K, in kJ/mol)

reaction	disproportionation	methyl shift isomerization
toluene[a]	179[b]	179
o-xylene[a]	164[c]	168
m-xylene[a]	174[c]	168[d]
		161[e]
p-xylene[a]	187[c]	171
benzene + CH_3-MOR → toluene + H-MOR	95	–
toluene + CH_3-MOR → *o*-xylene + H-MOR	86	–
toluene + CH_3-MOR → *m*-xylene + H-MOR	96	–
toluene + CH_3-MOR → *p*-Xylene + H-MOR	101	–

[a] Reaction catalyzed by H-MOR. [b] The disproportionation reaction leads to the formation of benzene and CH_3-MOR. [c] The disproportionation reaction leads to the formation of toluene and CH_3-MOR. [d] The product of this reaction is *o*-xylene. [e] The product of this reaction is *p*-xylene.

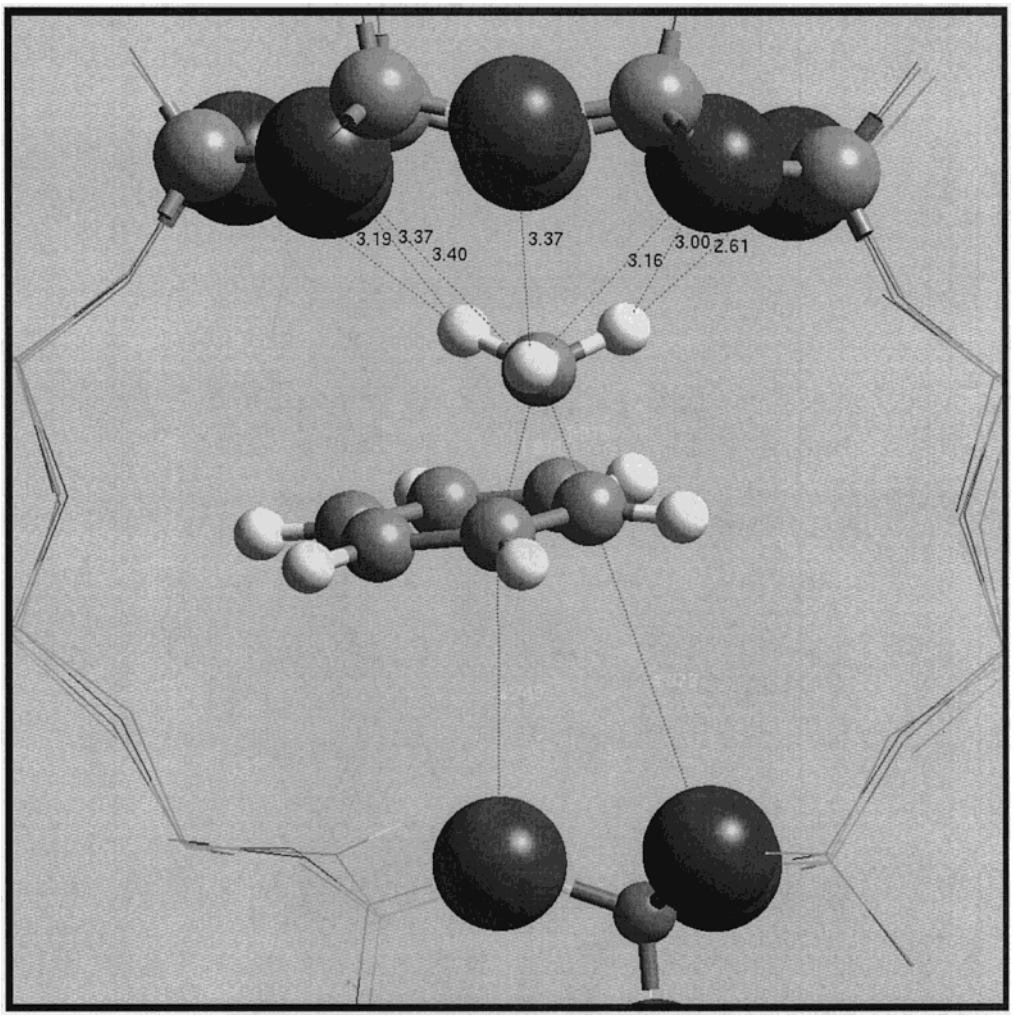

Figure 8. Detail of the geometry of the transition state **TS_shift_tol2**. The shifting methenium ion is in close interaction with the zeolitic oxygen atoms that belong to the 8-membered side pocket. These atoms are in the opposite side of the MOR 12-membered ring with respect to the Brønsted site. Distances are in Å.

The zeolite framework stabilization is very important for charged species or carbocationic transient species. Compared with[40] cluster approach data[16b] it is approximately 100 kJ/mol (35% of the activation energy in absence of zeolite framework electrostatic contribution). An estimate of the energy of the state equivalent to **C_tol2** was obtained in a previous cluster study. The energy of this species was +240 kJ/mol with respect to adsorbed toluene. **C_tol2** is +135 kJ/mol with respect to adsorbed toluene for the present periodic study. Again, the zeolite framework stabilization is about 100 kJ/mol. This is in agreement with the findings of Boronat et al.[42a] They concluded in a periodic embedding procedure study of charged species within a zeolite that the zeolitic electrostatic contribution uniformly shifts the energy levels of charged species downward, whereas neutral species energy levels remained unchanged. Neutral species are found in this study also to have energies similar to those calculated using a cluster approach. The phenoxy intermediate is +150 kJ/mol in this study, whereas it is +152 kJ/mol for the cluster approach method.[16b] However, in our present study the zeolite framework stabilization of charged species and transition states is energetically similar.

It has been previously mentioned that it is impossible to select a preferred reaction pathway. A lot of details have been given

(40) (a) Chen, Y.-H.; Hwang, L.-P. *J. Phys. Chem. B* **1999**, *103*, 5070–5080. (b) Waghmode, S. B.; Bharathi, P.; Sivasanker, S.; Vetrivel, R. *Microporous Mesoporous Mater.* **2000**, *38*, 433–443.

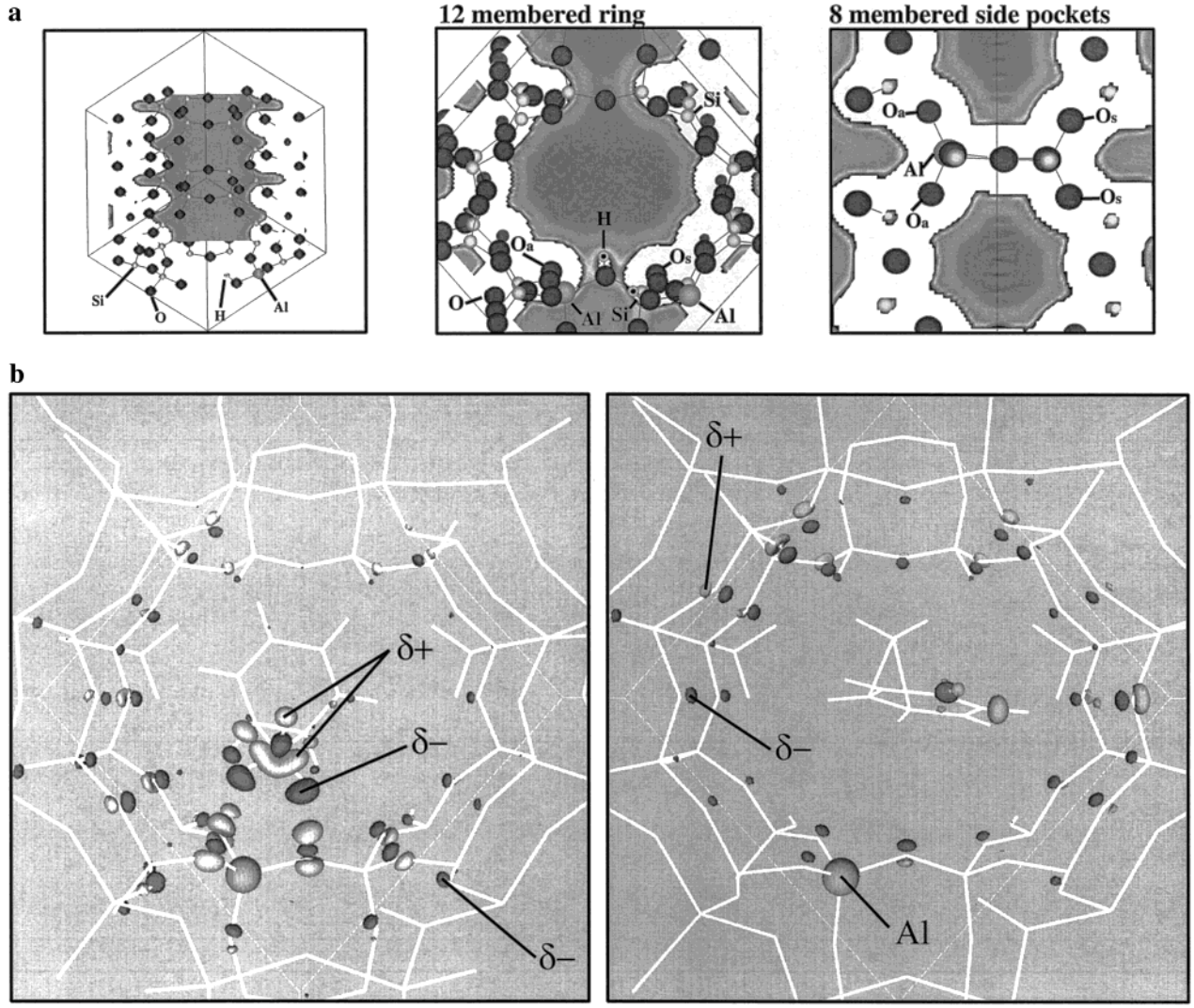

Figure 9. (a) Electron density cutting planes of acidic mordenite. The scale is not mentioned but respects a linear scaling of the data. The locations of aluminum and proton have been emphasized. It can be seen that electron density around Brønsted site oxygen atoms is only slightly more important than the electron density around other zeolitic oxygen atoms. (b) Polarization of the electronic density in **TS_shift_tol1** (left) and **TS_shift_tol2** (right). The polarization due to the transition states appears to affect all close-by zeolitic oxygen atoms.

for the reaction pathways of toluene. The most important one is that the isomerization transition states are the most demanding steps. Prior to the transition states, several nonstable intermediates have been found that can be considered as landmarks that characterize the differences among the three reaction pathways. They influence the choices of transition-state geometries. According to transition-state theory such intermediates do not have an influence on the transition state that will be preferred.[35,43]

Xylene Isomerization. The dispersion energy contribution has been calculated for all periodic geometries of xylene isomers. All dispersion energy data are within -95 ± 5 kJ/mol if the xylene species is *ortho*-, *meta*-, or *para*-xylene. Therefore, the periodic energies of the xylene molecules have been corrected with this single value.[44] The absence of an energy difference in xylene isomer adsorption energies has also been obtained by Deka et al.[31b] They performed classical dynamic simulations of xylene molecules adsorbed within various dealuminated zeolites, among which was mordenite.

The reaction energy diagrams of the isomerization reaction of xylene are depicted in Figure 10. Xylenes isomerization reaction activation energies are summarized in Table 9.

Concerning the isomerization reaction path via disproportionation, the order of the activation energies follows the same order as the hard−soft acid−base (HSAB) prediction for the methylation reaction of toluene catalyzed by zeolite.[45] The easiest methylation positions on toluene have been predicted to be *ortho* > *meta* > *para*. Vos et al.[22] have recently shown that this order can be affected by zeolite steric constraints. The aromatic molecules have enough space within the mordenite channels to avoid constraints on the transition states in the case of the disproportionation reaction of xylene molecules. Furthermore, the transition states that have been considered in this study are not characterized by topological restraints as in the case of the methylation reaction of toluene with methanol catalyzed by acidic zeolite. Therefore, the HSAB predicted order holds.

A different picture from that deduced from cluster calculations[16b] is obtained in the case of the shift isomerization reaction. Contrary to that observed in toluene isomerization reactions, the nonparticipating methyl group suffers from the close

(41) Ramachandran, S.; Lenz, T. G.; Skiff, W. M.; Rappé, A. K. *J. Phys. Chem.* **1996**, *100*, 5898−5907.

(42) (a) Boronat, M.; Zicovich-Wilson, C. M.; Corma, A.; Viruela, P. *Phys. Chem. Chem. Phys.* **1999**, *1*, 537−543. (b) Vollmer, J. M.; Truong, T. N. *J. Phys. Chem. B* **2000**, *104*, 6308−6312.

(43) Parmon, V. N. *Catal. Today* **1999**, *51*, 435−456.

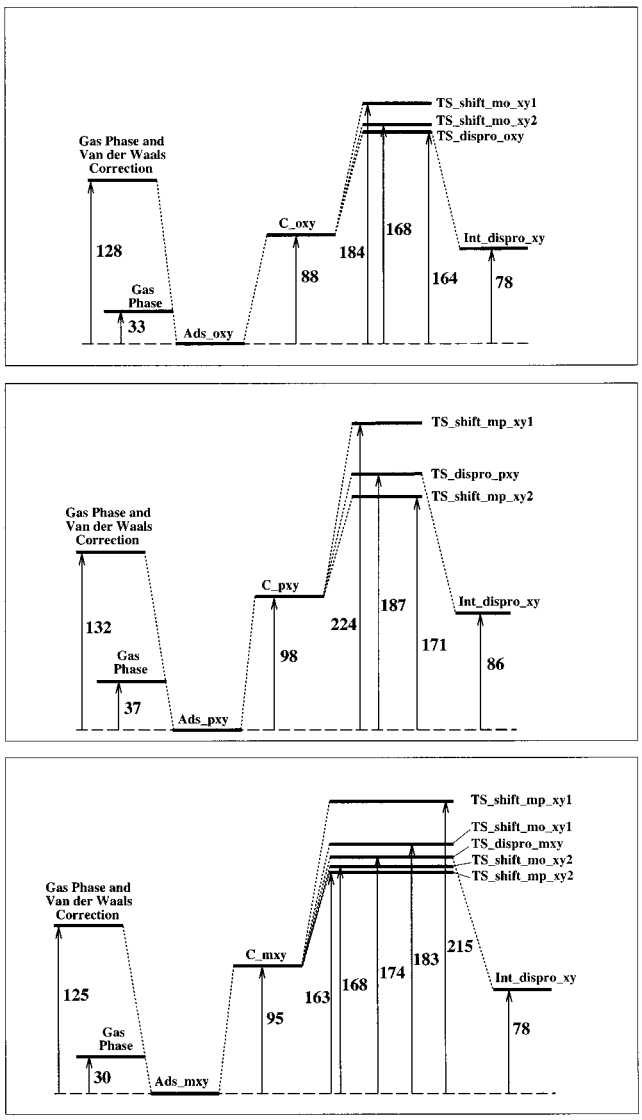

Figure 10. Reaction energy diagrams of *ortho*-xylene (top), *para*-xylene (middle), and *meta*-xylene (bottom) catalyzed by acidic mordenite. All values are in kJ/mol. The labels used in this Figure are the same as in Figures 5 and 6.

proximity to the zeolite wall in the xylene isomerization reaction. No difference for toluene activation energy was observed. Now differentiation occurs. It is particularly important for *meta*−*para*-xylene isomerization (see **TS__shift__mp__xy1** in Figure 5). In contrast, **TS__shift__mp__xy2** and **TS__shift__mo__xy2** do not show evidence of steric constraints. Their energy levels are lower or similar to that of disproportionation reaction transition states. Clearly, the xylene molecules reaction pathways that involve the shift isomerization mechanism for xylene, as predicted via cluster calculations, are disfavored. The activation energy differences are 16 and 53 kJ/mol for **TS__shift__mo__xy** and **TS__shift__mp__xy**, respectively. One can estimate that the shift isomerization reaction pathway occurs according to the shift isomerization which follows the protonation step without further reorientation of xylene.

The reaction energy diagram of *ortho*-xylene isomerization reactions indicates that competition exists between shift isomerization and isomerization via disproportionation reaction mechanisms. The difference between the activation energies is only 2 kJ/mol. For *meta*-xylene and *para*-xylene, shift isomerization is preferred. The differences in activation energies are 11 and 16 kJ/mol respectively in favor of the shift isomerization reaction pathway. The *meta*-xylene isomerization reactions lead as easily to *ortho*-xylene ($E_{act} = +168$ kJ/mol) as to *para*-xylene ($E_{act} = +163$ kJ/mol). Similarly, isomerization reactions of *ortho*-xylene and *para*-xylene are equally difficult to achieve (E_{act}'s are +164 and +171, respectively). Regarding these results, no transition-state selectivity is predicted for xylene isomerization reactions catalyzed by acidic mordenite (see Table 9).

The evaluation of the apparent activation energies using eq 2 gives data between +40 to +100 kJ/mol for Θ between 0 and 0.5 ($^{app}E_{act} = +36$, +40, and +39 kJ/mol for *ortho*-xylene, *meta*-xylene, and *para*-xylene and $\Theta = 0$). These are in very good agreement with experimental data that have been reported to be around 40 kJ/mol.[15b,46]

5. Conclusions

In this theoretical study we have shown how a combination of steric constraints and electrostatic contributions of zeolitic atoms can affect the reaction pathways of intramolecular isomerization reactions of toluene and xylene isomers. Isomerization reactions may proceed according to different reaction pathways which do not show energetic differences in the absence of steric constraints. It has been observed that zeolitic channel oxygen atoms play an important role in the stabilization of the transition states. The location of the transition sates with respect to the Brønsted site can be altered completely if the zeolitic topology allows a more efficient way to stabilize the transient species. Apart from this, the reaction mechanisms obtained via the cluster approach and periodic calculations remain, in essence, similar. Small cluster calculations have been proven to give good qualitative results compared with periodic results. Differences result from the fact that zeolitic micropore oxygen atoms are not passive spectators but rather participate actively in the catalysis of reactions. The contribution of the zeolitic oxygen atoms appears to be of short-range nature.

The presence of steric constraints has been shown to inhibit the possibility that isomerization of toluene and xylene proceed via some reaction pathways. Destabilization of transition states is up to 50 kJ/mol although aromatics can fit without difficulty inside the mordenite large pores. Steric constraints are strongly dependent on the transition-state structure as well as on the zeolite topology.[47]

The results obtained in this study provide with a new insight in solid acid heterogeneous catalysis. A good agreement has been obtained with experimental data.

Acknowledgment. Computational resources have been partly granted by the Dutch National Computer Facilities (NCF). This work has been performed within the European Research Group "Ab Initio Molecular Dynamics Applied to Catalysis", supported by the Centre National de la Recherche Scientifique (CNRS), the Institut Français du Pétrole (IFP), and the TotalFinaElf Raffinage Distributions company. X.R. thanks TotalFina Raffinage Distributions for the support, and C. G. M. Hermse for the fruitful discussions.

JA0103795

(44) The van der Waals energy corrections are −98, −96, −99, −100, −97, −96, −95, −100, −94, −93, and −96 kJ/mol for **Ads__oxy**, **Ads__mxy**, **Ads__pxy**, **TS__shift__mo__xy1**, **TS__shift__mo__xy2**, **TS__dispro__oxy**, **TS__shift__mp__xy1**, **TS__shift__mp__xy2**, **TS__dispro__pxy**, and **TS__dispro__mxy**, respectively.

(45) Corma, A.; Llopis, F.; Viruela, P.; Zicovich-Wilson, C. *J. Am. Chem. Soc.* **1994**, *116*, 134−142.

(46) Norman, G. H.; Shigemura, D. S.; Hopper, J. R. *Ind. Eng. Chem., Prod. Res. Dev.* **1976**, *15*, 41−45.

(47) Sponer, J.; Sponer, J.; Cejka, J.; Wichterlava, B. *J. Phys. Chem. B* **1998**, *102*, 7169−7175.